Received: 1 May 2020 | Revised: 8 June 2020 | Accepted: 22 June 2020

DOI: 10.1002/bit.27474

ARTICLE

BIOTECHNOLOGY BIOENGINEERING WILEY

Aggregation-induced integrated stress response rejuvenates culture-expanded human mesenchymal stem cells

Brent M. Bijonowski[1,4] | Qin Fu[1,5] | Xuegang Yuan[1,2] | Jerome Irianto[3] | Yan Li[1] | Samuel C. Grant[1,2] | Teng Ma[1]

[1]Department of Chemical and Biomedical Engineering, FAMU-FSU College of Engineering, Florida State University, Tallahassee, Florida

[2]The National High Magnetic Field Laboratory, Florida State University, Tallahassee, Florida

[3]Department of Biomedical Sciences, College of Medicine, Florida State University, Tallahassee, Florida

[4]University of Münster, Münster, Germany

[5]Proteomics Center, Cornell University, Ithaca, New York

Correspondence
Brent M. Bijonowski and Yan Li, Florida State University, 2525 Pottsdamer St., Tallahassee, FL 32310.
Email: bmb14d@my.fsu.edu (B. M. B.) and yli4@fsu.edu (Y. L.)

Funding information
National Science Foundation of USA, Grant/Award Number: 1743426; National Institutes of Health of USA, Grant/Award Number: R01NS102395-01A1

Abstract

Protein homeostasis is critical for cellular function, as loss of homeostasis is attributed to aging and the accumulation of unwanted proteins. Human mesenchymal stem cells (MSCs) have shown promising therapeutic potential due to their impressive abilities to secrete inflammatory modulators, angiogenic, and regenerative cytokines. However, there exists the problem of human MSC expansion with compromised therapeutic quality. Duringin vitro expansion, human MSCs are plated on stiff plastics and undergo culture adaptation, which results in aberrant proliferation, shifts in metabolism, and decreased autophagic activity. It has previously been shown that three-dimensional (3D) aggregation can reverse some of these alterations by heightening autophagy and recovering the metabolic state back to a naïve phenotype. To further understand the proteostasis in human MSC culture, this study investigated the effects of 3D aggregation on the human MSC proteome to determine the specific pathways altered by aggregation. The 3D aggregates and 2D cultures of human MSCs derived from bone marrow (bMSC) and adipose tissue (ASC) were analyzed along with differentiated human dermal fibroblasts (FB). The proteomics analysis showed the elevated eukaryotic initiation factor 2 pathway and the upregulated activity of the integrated stress response (ISR) in 3D aggregates. Specific protein quantification further determined that bMSC and ASC responded to ISR, while FB did not. 3D aggregation significantly increased the ischemic survival of bMSCs and ASCs. Perturbation of ISR with small molecules salubrinal and GSK2606414 resulted in differential responses of bMSC, ASC, and FB. This study indicates that aggregation-based preconditioning culture holds the potential for improving the therapeutic efficacy of expanded human MSCs via the establishment of ISR and homeostasis.

KEYWORDS

aggregates, eIF2 pathway, homeostasis, integrated stress response, mesenchymal stem cells, proteomics

Brent M. Bijonowski and Qin Fu are co-first authors.

This article is in memoriam of Dr. Teng Ma, who unexpectedly passed away on May 18, 2019 due to heart attack.

1 | INTRODUCTION

Human mesenchymal stem cells (MSCs) are the most clinically studied cell type for stem cell-based therapies worldwide and hold promises in treating various diseases (Fung, Yuan, Atkins, Shi, & Bubela, 2017). As stromal cells, MSCs occupy a regenerative niche in the stromal layer throughout the body and can be readily isolated from various tissue sources and expanded in culture (Chamberlain, Fox, Ashton, & Middleton, 2009). Although MSCs are partially defined by their multilineage differentiation potential, most significantly, it is their trophic functions that contribute to the therapeutic outcomes (Galipeau & Sensebe, 2018). Extensive in vitro studies have shown that MSCs are highly responsive to both biomechanical and biochemical cues, and have short-term mechanical and immune "memories" as well as the capacity to regulate cell fate and secretion of trophic and bioactive factors (Bijonowski, Daraiseh, Yuan, & Ma, 2019; Das, Gocheva, Hammink, Zouani, & Rowan, 2016; Diaz et al., 2017; Murphy, Moncivais, & Caplan, 2013; Song et al., 2017). However, maintaining innate properties of MSCs during large-scale expansion and identifying an optimal cell delivery strategy remain significant challenges in MSC clinical translation (Galipeau & Sensebe, 2018; Garcia-Prat et al., 2016; Yin, Zhu, & Ankrum, 2019).

Environmental responsiveness of MSCs is adversely influenced by cell source as well as in vitro expansion systems (Bazhanov et al., 2016; Khong et al., 2018; Wang, Chen, Cao, & Shi, 2014). Expansion of MSCs on stiff two-dimensional (2D) surfaces generates a heterogeneous cell population, which significantly reduces cell survival and secretion of immunomodulatory factors, and results in compromised therapeutic outcomes (Banfi et al., 2000; Bianco, Robey, Saggio, & Riminucci, 2010; Garcia-Prat et al., 2016; Yin et al., 2019). For example, in graft-versus-host disease, the 1-year survival rate for patients receiving MSCs at Passages 1–2 was 75%, while at Passages 3-4 it was reduced to 21% (von Bahr et al., 2012). To overcome these limitations, priming MSCs via different signals such as hypoxia, matrix mechanics, and cytokines have been employed to preserve stem cell characteristics based on the sensitivity of MSCs to specific stimuli (Yin et al., 2019). In particular, 3D aggregation of MSCs has been shown as a promising preconditioning strategy (Sart et al., 2020; Sart, Tsai, Li, & Ma, 2014), which can restore phenotypic properties of MSCs, promote the secretion of cytokines, and enhance the therapeutic potential of MSCs (Costa, McDevitt, Cabral, da Silva, & Ferreira, 2017; Liu, Munoz, Tsai, Logan, & Ma, 2017; Pennock et al., 2015; Wobma, Liu, & Vunjak-Novakovic, 2018). To date, however, the underpinning mechanism for aggregation-mediated functional enhancement of MSCs remains to be fully understood.

The integrated stress response (ISR) is an elaborate adaptive pathway that enables eukaryotic cells to maintain cellular homeostasis in response to both intrinsic and extrinsic stress factors such as accumulation of unfolded proteins, nutrient starvation, and viral infection (Pakos-Zebrucka et al., 2016). The core regulatory event in ISR is the phosphorylation of eukaryotic translation initiation factor 2 alpha (eIF2α) by stress-induced eIF2α kinases, which causes a reduction in global protein synthesis while directing a number of transcriptional mechanisms that regulate cell survival, restore cellular homeostasis, or activate apoptosis (Lu, Harding, & Ron, 2004). ISR plays an important role in maintaining cellular homeostasis along with phenotypic and functional properties in adult stem cells. For example, hematopoietic stem cells maintain life-long proliferation, integrity of the blood system, and enhance survival in the presence of nutrient deprivation by modulating ISR activity (van Galen et al., 2018). A recent study has shown that the higher basal level of ISR was found in induced pluripotent stem cell-derived cardiac progenitor cells compared to mature cardiomyocytes, which is the key to maintain cellular integrity in cardiac progenitors and preventing differentiation of damaged cells (Searfoss, Paisley, Goldstein, Baker, & Willy, 2019). Though the ISR is widely acknowledged for regulating cellular homeostasis, its role in MSC culture expansion and preconditioning is yet to be reported.

This study sets out to test the hypothesis that ISR plays a key role in maintaining protein homeostasis and functional response of MSCs. To test this hypothesis, proteomic analysis was performed for human bone marrow-derived MSCs (bMSCs), human adipose tissue-derived MSCs (ASCs), and dermal fibroblasts (FBs) in standard 2D adherent and 3D aggregate cultures. Protein analysis demonstrated a shift in the eIF2 pathway following the aggregation of bMSCs and ASCs. Further analysis of specific proteins by western blot validated the label-free proteomics analysis and showed that increased phosphorylation of eIF2α led to decreased protein synthesis following aggregation. The role of ISR was further connected to stemness and autophagy by western blot analysis using small molecules to perturb the eIF2 pathway. ISR-induced functional enhancement was examined via ischemic survival analysis, which demonstrated that bMSC and ASC aggregates were less susceptible to ischemia. Taken together, these results illustrate a new homeostatic state established by the activation of ISR in bMSCs and ASCs following aggregation, which is not found in fibroblasts. The results indicate that human MSC aggregation increases ISR activity which should lead to improved proteome control and therapeutic function of MSCs.

2 | MATERIALS AND METHODS

2.1 | Culture of ASCs, bMSCs, and fibroblasts

Frozen ASCs and bMSCs at Passage 1, in liquid nitrogen, were obtained from the Tulane Center for Stem Cell Research and Regenerative Medicine. Fibroblasts were purchased from American Type Culture Collection (Manassas, VA) at Passage 1. The ASCs were isolated from the liposate of deidentified healthy donors (at age range of 39–43 years old) and bMSCs from deidentified healthy bone marrow (at age range 21–33 years old). All cells were expanded with minimum essential medium-α (Life Technologies, Carlsbad, CA) supplemented with 1% penicillin/streptomycin (Life Technologies) and 10% fetal bovine serum (FBS; Atlanta Biologicals, Lawrenceville, GA) as complete culture media (CCM) on 150-mm tissue culture Petri dishes (Corning, Corning, NY) to a density of ~1,500 cells/cm^2 in a standard 5% CO_2 incubator.

The culture media was changed every 3 days. Cells of Passages 4–6 were used in this study. All culture reagents were purchased from Sigma-Aldrich (St. Louis, MO) unless otherwise noted.

2.2 | Aggregate formation

Once cells reached 90% confluence, the cells were trypsinized and pelleted. The pellet was resuspended in CCM to a final concentration of 2.5×10^5 cells/ml. For 3D aggregation, the cell suspension (1 ml) was pipetted into each well of an ultralow attachment (ULA) 6-well plate for a total of 1.5×10^6 cells. The aggregates were homogenized for 48 hr. Multiple aggregates were observed in each well. For parallel 2D control cultures, the cells were seeded for a total of 8×10^5 cells in 150-mm tissue culture Petri dishes at the same time and cultured for 48 hr. Three-dimensional aggregates were collected and 2D cultures were harvested by trypsinization after 48 hr for proteomics analysis and western blot. Considering a roughly 30% of cell loss in the 3D aggregation after 48 hr and the cell growth in 2D cultures, the cultures generated a similar cell number at the harvest point (~1×10^6 cells/sample). The morphologies and size-distribution of aggregates (100–400 μm in diameter) can be tracked and imaged with an Olympus IX70 microscope (Center Valley, PA) and were reported in our previous publication (Tsai, Liu, Yuan, Chella, & Ma, 2017). For some experiments, the cultures were treated with 2-aminoethoxydiphenyl borate (2-APB, 100 μM; Sigma-Aldrich) or Thapsigargin (Thap, 1 μM; Sigma-Aldrich) to study the effects of biomechanical force on ISR. 2-APB prevents transient receptor potential (TRP) channel Ca^{2+} flux, and Thap is a sarcoendoplasmic reticulum calcium transport ATPase (SERCA) agonist which induces endoplasmic reticular calcium release.

2.3 | Protein extraction and digestion

Protein extraction was carried out according to Figure 1a. In brief, three independent biological replicates were harvested from both 2D adherent plates (80% confluence) and ULA plates (48 hr for self-assembly). Samples were washed with ice-cold phosphate buffer saline (PBS) three times, scrapped, and pelleted (5 min at 500 g). Samples were resuspended in a mixture of 8 M urea, 50 mM ammonium bicarbonate, and protease inhibitor cocktail (Sigma-Aldrich). Cells were homogenized with a Sonic Dismembrator 100 (Thermo Fisher Scientific, Hampton, NJ), and the concentration of protein was determined by the Bradford assay (Bio-Rad, Hercules, CA) according to the manufacturer's instructions. Extracted proteins were digested by a modified filter-aided sample preparation method (Wisniewski, Zougman, Nagaraj, & Mann, 2009). Briefly, 100 μg of protein was vacuum dried and resuspended in 8 M urea to a final volume of 200 μl, then 10 mM dithiothreitol, and 50 mM iodoacetamide were added for reduction and alkylation, respectively. After that, the sample was transferred to a 10 kDa filter and centrifuged at 14,000 g for 30 min to remove the solvent. The sample was then washed with 200 μl of 8 M urea and 200 μl of ammonium bicarbonate and centrifuged at 14,000 g for 30 min. The supernatant was discarded and 2 μg trypsin was added for digestion at 37°C overnight. The peptides were collected and vacuum-desiccated for further analysis.

2.4 | Liquid chromatography-tandem mass spectrometry

For liquid chromatography-tandem mass spectrometry (LC-MS/MS) experiments, three biological samples were prepared for each cell type and condition (bMSC in 2D and 3D, ASC in 2D and 3D, and FB in 2D and 3D). An externally calibrated Thermo Q Exactive HF (high-resolution electrospray tandem mass spectrometer) was used in conjunction with Dionex UltiMate 3000 RSLCnano System for the purpose of parsing the peptides. The solution of 1 μg of peptides in 0.1% formic acid was aspirated into a 50 μl loop and loaded onto the trap column (Thermo μ-Precolumn 5 mm, with nanoViper tubing 30 μm id × 10 cm). The flow rate was set to 300 nl/min for separation on the analytical column (Acclaim PepMap RSLC 75 μM × 15 cm nanoViper). Mobile phase A was composed of 99.9% H_2O with 0.1% formic acid while mobile phase B was composed of 99.9% acetonitrile with 0.1% formic acid. A 120-min-stepped gradient from 3% to 45% B was performed. The liquid chromatography eluent was directly nanosprayed into the Q Exactive HF mass spectrometer (Thermo Fisher Scientific). During the chromatographic separation, the Q Exactive HF was operated in a data-dependent mode and under the direct control of the Thermo Excalibur 3.1.66 (Thermo Fisher Scientific). The MS data were acquired using the following parameters: 20 data-dependent collisional-induced-dissociation MS/MS scans per full scan (m/z = 350–1700). LTQ spray voltage was 2.0 kV and the capillary temperature was set at 200°C. A survey full scan (m/z = 350–1700) and the five most intense ions were selected for a zoom scan to determine the charge state, after which MS/MS was triggered in Pulsed-Q Dissociation mode with minimum signal required (1,000), isolation width 2.0, normalized collision energy 27.0.

2.5 | Proteomics data analysis

Raw data files were collected from the client software and analyzed by MaxQuant 1.6 (Max-Plank Institute, Munich, Germany) followed by Scaffold 4.4 (Proteome Software, Portland, OR). Differentially expressed proteins (DEPs) were identified and filtered based on two or more unique peptides with a 95% confidence interval. Benjamini–Hochberg false discovery rate (FDR) control threshold of 0.05 was applied to further filter the proteins based on a two-tailed *t* test during the quantification process. Principle component analysis (PCA) was performed to reduce the redundancy of related data properties and summarize the data using the best linear combinations by Perseus software (Computational Systems Biotechnology, Munich, Germany). Canonical pathway analysis was performed using Ingenuity Pathway Analysis (IPA) software (Qiagen, Redwood City, CA; http://www.ingenuity.com).

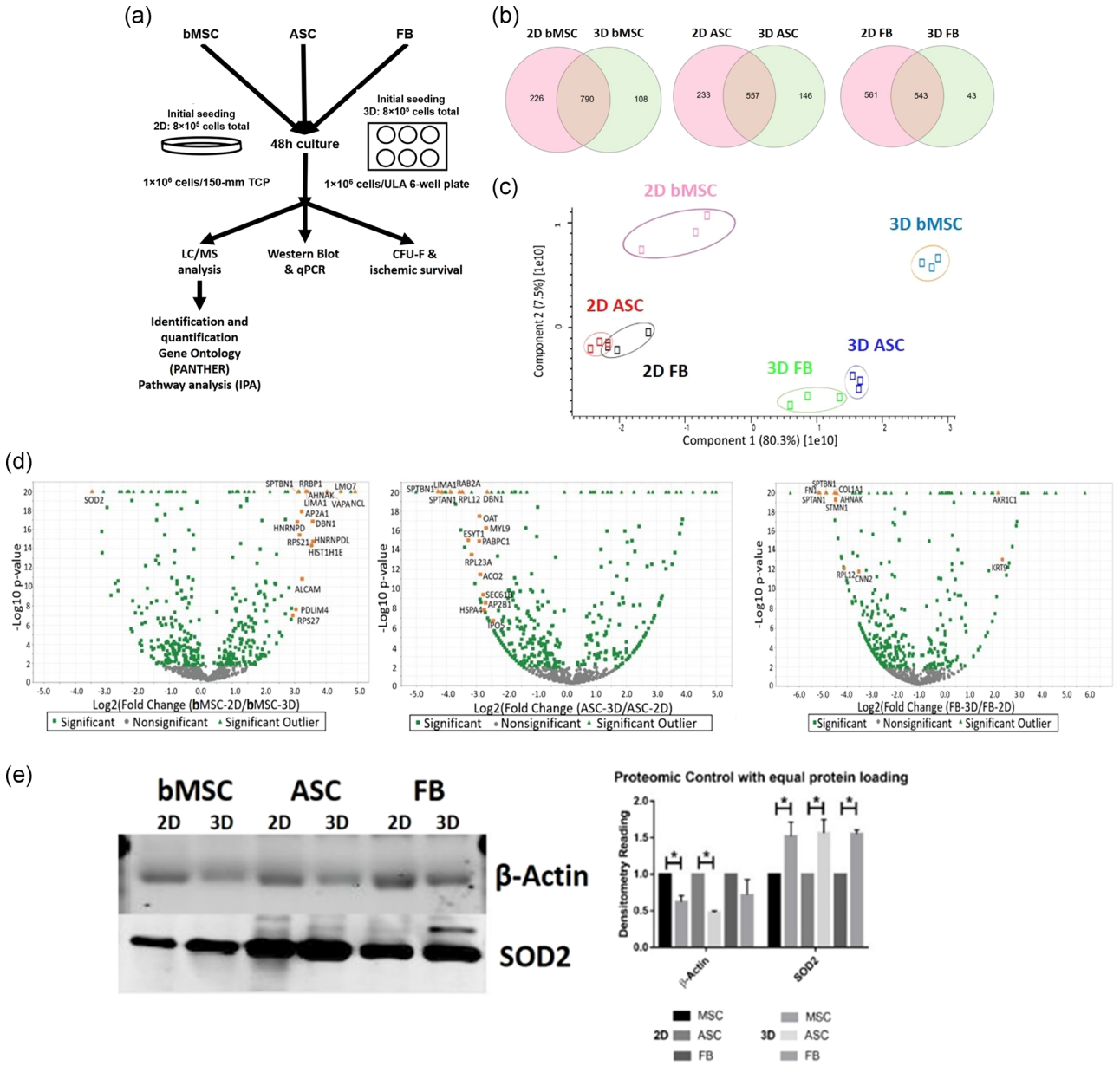

FIGURE 1 Quantification of differentially expressed proteins (DEP) found in human bone marrow-derived mesenchymal stem cells (bMSCs), human adipose tissue-derived mesenchymal stem cells (ASCs), and dermal fibroblasts (FBs). (a) Schematic of proteomics experiments, which involved three biological repeats for each cell line. (b) Venn diagram plots for DEPs show hundreds of identified proteins, and hundreds of shared DEPs in the planar (2D) and aggregated (3D) conditions. (c) PCA plots of conditions and groups reveal that planar and aggregated cells are distinctly separated on the axis of highest variability. (d) Volcano plots illustrate the number of significant DEPs within the hundreds of DEPs. Orange color symbols indicate the proteins with more than 10-fold change following aggregation. The enlarged volcano plots were shown in Figure S1. (e) Western blot analysis validates the accuracy of proteomics data; two proteins (SOD2 and β-actin) were selected for the validation. Data represent the mean of at least three independent determinations; errors represent the standard error in the mean. 2D, two-dimensional; PCA, principal component analysis; SOD2, superoxide dismutase 2. *$p < .05$ [Color figure can be viewed at wileyonlinelibrary.com]

2.6 | Western blot assay

Aggregates and planar cells were washed with PBS, and lysed in radioimmunoprecipitation assay buffer (150 mM sodium chloride, 1.0% Trition X-100, 0.5% sodium deoxycholate, 0.1% sodium dodecyl sulfate, 50 mM Tris, pH 8, 2 μg/ml Aprotinin, 5 μg/ml Leupeptin, 5 μg/ml Antipain, 1 mM phenylmethylsulfonyl fluoride protease inhibitor), and homogenized by sonification using a Sonic Dismembrator 100 (Thermo Fisher Scientific). Samples were then digested for 20 min on ice, and spun down at 14,000 rpm for 20 min. The supernatant was collected and a Bradford assay was carried out to determine the protein concentration. Protein lysate concentration was normalized, and 20 μg of each sample was denatured at 95°C in 2× Laemmli Sample buffer. Proteins were separated by 15% BIS-Tris-SDS gels and transferred onto

a nitrocellulose membrane (Bio-Rad). For the detection of nonphosphorylated proteins, the membranes were blocked for 30 min in 3% skim milk (wt/vol) in Tris-buffered saline (10 mM Tris-HCl, pH 7.5, and 150 mM NaCl) with 0.1% Tween 20 (vol/vol; TBST), or in 3% bovine serum albumin in TBST. Membranes were incubated overnight in the presence of the primary antibody diluted in the corresponding blocking buffer at 4°C. Afterward, the membranes were washed four times for 10 min each with TBST and then incubated with an IR secondary (LI-COR, Lincoln, NE) at 1:10,000 for 180 min at room temperature. Blots were washed another four times for 10 min each with TBST and processed using the LI-COR Odyssey (LI-COR). Images were analyzed using the ImageJ software for band density, and the band density of proteins of interest was normalized to the band density of endogenous control α-tubulin.

2.7 | Real-time reverse transcriptase-polymerase chain reaction analysis

Aggregate or planar culture pellets were homogenized with a Sonic Dismembrator 100 (Thermo Fisher Scientific) and total RNA was extracted using an RNeasy Mini Kit (Qiagen, Valencia, CA). RNA (2 μg) was used to carry out reverse transcription, with anchored oligo-dT primers (Operon, Louisville, KY) and Superscript III (Invitrogen, Grand Island, NY). Specific primers for target genes were designed in the software Oligo Explorer 1.2 (Genelink, Hawthorne, NY). Vinculin was used as an endogenous control for normalization. Reverse transcriptase-polymerase chain reaction (RT-PCR) reactions were performed on an ABI7500 instrument (Applied Biosystems, Foster City, CA), using SYBR Green PCR Master Mix. After amplification, the quality and primer specificity were verified. Variation in gene expression was evaluated using the comparative C_t method: $2^{-(\Delta C_{t\,\text{treatment}} - \Delta C_{t\,\text{control}})}$, based on the expression of the target gene (normalized to vinculin).

2.8 | Ischemic culture and measurement of caspase 3/7 activity

MSCs were divided into two groups: control and ischemic. Control cells were cultured under standard carboxygen with serum, while ischemic cells were placed in a hypoxia chamber (2% oxygen), and fed with CCM without FBS. After overnight culture, cells in each group were processed for measuring DNA content to determine cell number, and for measuring caspase 3/7 activity. Caspase 3/7 activity assay was carried out according to the manufacturer's instructions (Bio-Rad). DNA content was determined using picogreen as previously described (Bijonowski et al., 2019).

2.9 | Colony-forming unit assay

Cells were cultured in CCM at 12 cells/cm^2. Small-molecule inhibitors salubrinal (5 μM) and GSK-2606414 (10 μM) were added to evaluate ISR response on colony formation along with no treatment control. Cells were cultured in a 5% CO_2 incubator at 37°C for 14 days. The cells were then washed three times with PBS and stained with 0.5% crystal violet (in methanol) for 5 min. After washing, the numbers of colonies were counted.

2.10 | Statistics

A two-tailed Student's *t* test was used to compare two groups, and for multiple group comparison, a one-way analysis of variance with Tukey's host hoc analysis was performed using SPSS software (Chicago, IL; http://www.spss.com). All data are presented as a mean value with standard deviation (mean ± *SD*). Differences were considered to be statistically significant when the *p* values were <.05.

3 | RESULTS

3.1 | Proteomics analysis for protein identification

Proteomics data were collected from the LC-MS/MS and the amino acids were reviewed against the human proteome database of Swiss-Prot with an FDR < 5% and a minimum of two unique peptides per protein. A total of 1,124, 936, and 1,147 different proteins were identified for bMSC, ASC, and FB groups, respectively. A total of 790 proteins (70.3%) overlapped between 2D and 3D conditions for bMSCs, 557 proteins were in common for ASCs (59.5%), and 543 common proteins were found for the FB group (47.3%; Figure 1b). Next, the Benjamini–Hochberg procedure was utilized to define the cutoff components in PCA, which in turn showed significant separation between 2D and 3D conditions for each cell type (Figure 1c). Volcano plots of the proteomics data revealed the proteins with more than 10-fold change following aggregation: superoxide dismutase (SOD2), nucleolin, 40S ribosomal protein S27 in bMSCs, spectrin alpha chain, nonerythrocytic 1 (SPTAN1), spectrin beta chain, nonerythrocytic 1, LIM domain, and actin-binding protein 1 in ASCs, and aldo-keto reductase family 1 member C1, spectrin alpha chain, nonerythrocytic 1 (SPTAN1), fibronectin 1 in FBs (Figures 1d and S1). Following the Benjamini–Hochberg procedure, the analysis of 3D samples versus 2D samples highlighted 246, 197, and 195 proteins enriched at least twofold in bMSCs, ASCs, and FBs, respectively. Of these, the two differentially expressed proteins β-actin and SOD2 were selected for validation of proteomics results by western blot. Consistent trends in the expression of β-actin and SOD2 were observed in comparison with proteomics results of 2D and 3D samples for each cell type (Figure 1e).

3.2 | Pathway analysis of differentially expressed proteins

Canonical pathway analysis of the identified DEPs was performed by IPA, which demonstrated the top five enriched categories of canonical

pathways with a p value less than 10^{-5} in all three cell types (Figure 2a). Specifically, for bMSCs, DEPs were enriched in eIF2 signaling, regulation of eIF4 and p70S6K signaling, protein ubiquitination pathway, the mammalian target of rapamycin (mTOR) signaling, and phagosome maturation. For ASCs, DEPs were enriched in eIF2 signaling, regulation of eIF4 and p70S6K signaling, remodeling of epithelial adherens junctions, mTOR signaling, and regulation of actin-based motility by Rho. For FBs, DEPs were primarily enriched in eIF2 signaling, regulation of eIF4 and p70S6K signaling, mitochondrial dysfunction, mTOR signaling, and unfolded protein response. Since the eIF2 pathway was enriched, further analysis was performed by IPA. The results indicate that eIF2α was downregulated in bMSC and ASC aggregates, but not in FB aggregates as shown in the schematic interactions of specific proteins in the eIF2 pathway (Figure 2b). As the donors of bMSCs and ASCs are deidentified and randomized, no connection of the ISR with donor demographics can be found. Therefore, the differential ISR expression is highly likely related to cellular phenotype of the cells when grown as 3D aggregates or 2D monolayers.

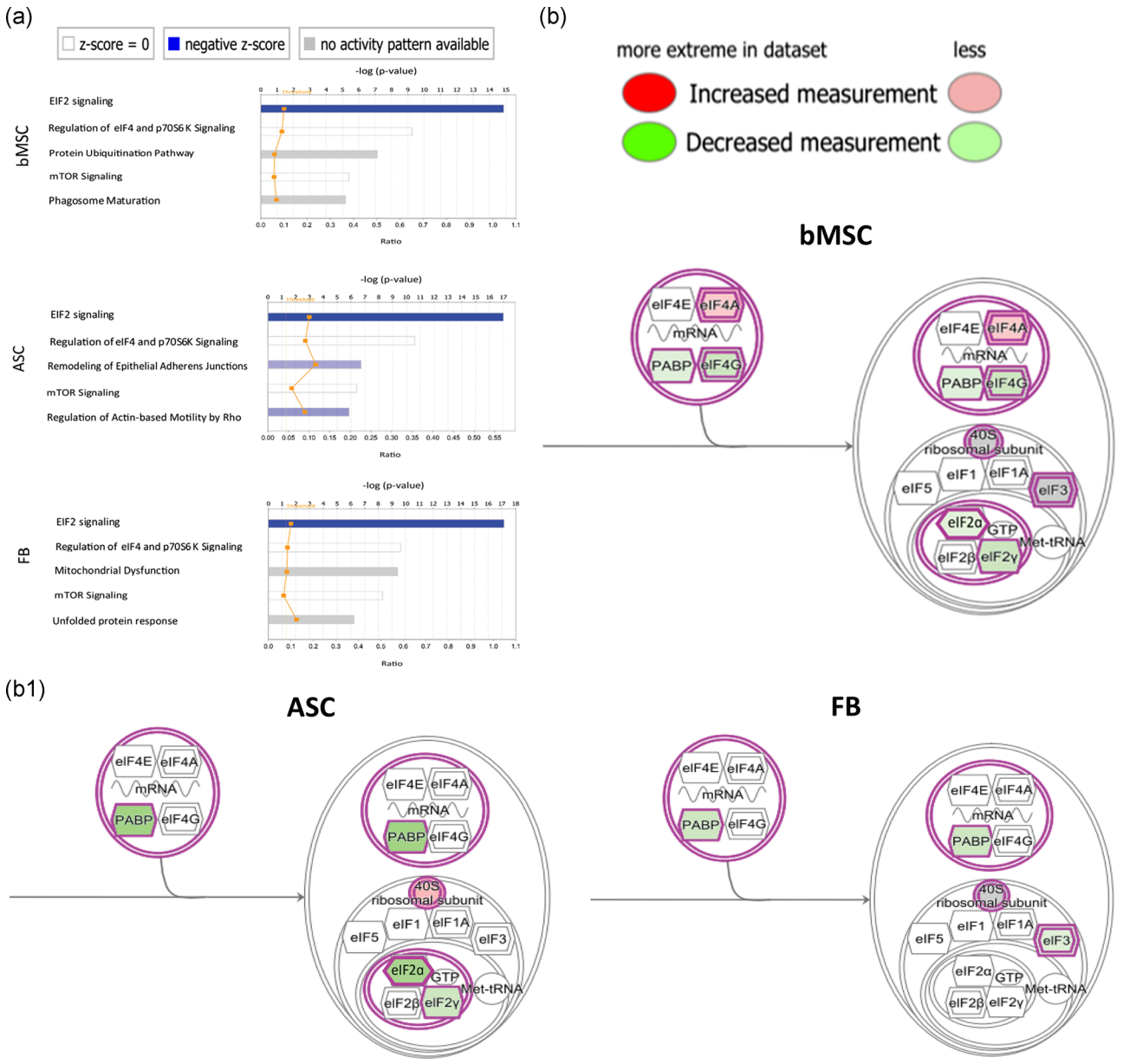

FIGURE 2 Evaluation of proteomics data to reveal significant pathways and proteins. (a) Canonical pathway analysis reveals the top five pathways altered by aggregation. (b) Ingenuity pathway analysis (IPA) of the most significant pathways revealed protein patterns, which were responsible for the observed effect. Ratio: the number of proteins in our data set versus the number of proteins in this pathway. The three illustrations in (b) have the same proteins and flow chart, but the color of the box indicates different expression levels as shown in the color scale. For example, red color shows more increased measurement, while pink color shows less increased measurement. The dark green color shows more decreased measurement, while the light green color shows less decreased measurement [Color figure can be viewed at wileyonlinelibrary.com]

3.3 | Analysis of the three principal parts of ISR

Selected DEPs involved in ISR were plotted as genome heatmap with hierarchical cluster analysis (Figure 3). Analysis of the recognized DEPs revealed that both bMSCs and ASCs had more DEPs involved in the formation of preinitiation complex (Figure 3a), which would potentially result in a significant alteration of ISR in these two cell types, but not in FB. Next, the chaperones were separately plotted, and similar trends were observed for the three cell types in the context of ISR alteration. It was noted that the FB group had an increased level of HSPA5, which is a potent regulator of the eIF2 pathway (Figure 3b). Finally, a higher number of proteasome proteins was found in bMSCs and ASCs than the FB group (Figure 3c). IPA was also performed for the involvement of DEPs in potential diseases and functions, which indicate that protein synthesis, cell death and survival, and RNA damage and repair were the top three dominating categories enriched in for the three cell types (Figure S2).

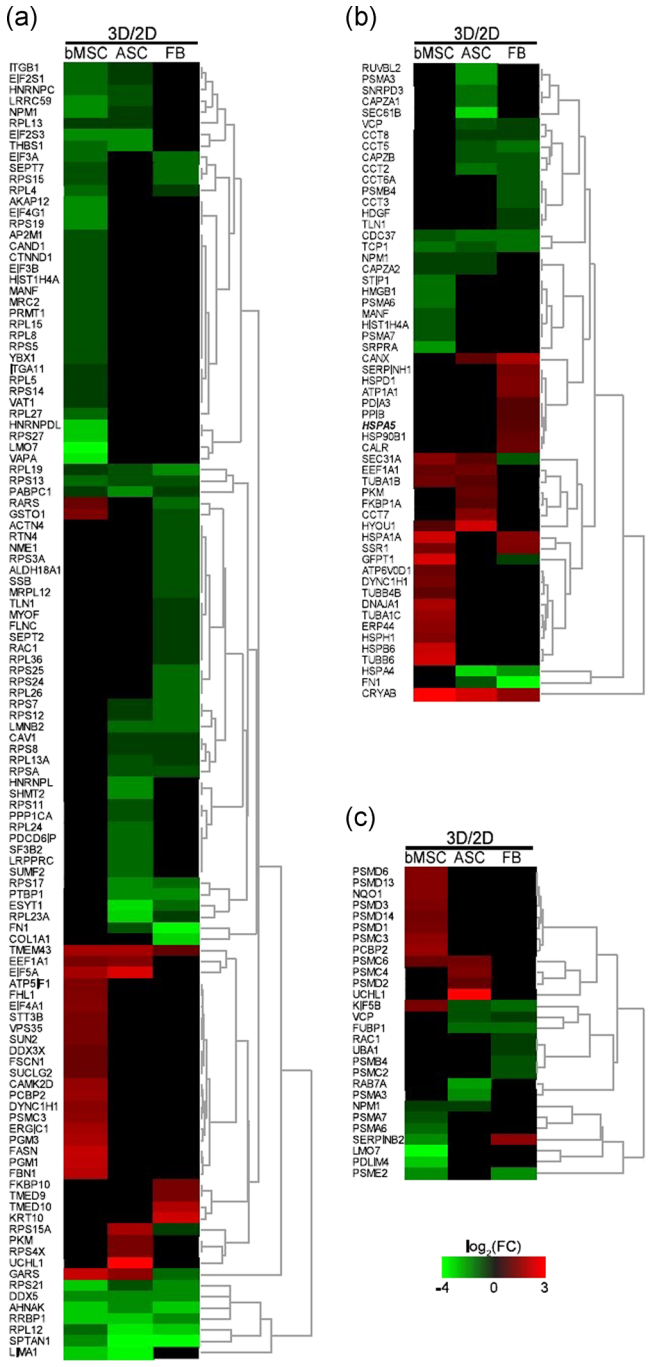

FIGURE 3 Heat maps of the three principal parts of the integrated stress response to misfolded proteins. (a) Proteins responsible for control over the preinitiation complex. (b) Chaperone proteins responsible for either refolding a misfolded protein or coating the protein for ubiquitination. (c) Proteins of the proteasome complex [Color figure can be viewed at wileyonlinelibrary.com]

3.4 | Protein-based assessment of the ISR following aggregation

To understand the different activation of eIF2 pathways based on the results of IPA, the proteins involved in eIF2 phosphorylation and dephosphorylation as well as the downstream autophagy cascade (Figure 4a) were investigated using western blot. Analysis of the upstream kinase revealed the increased expression of protein kinase R-like endoplasmic reticulum kinase (PERK) and p-PERK in 3D aggregates compared to 2D cells for bMSCs and ASCs, while no difference was observed for the FB group (Figure S3a). The increased ratio of phosphorylation to total PERK indicated that eIF2 signaling was activated in 3D aggregates compared to 2D cells (Figure 4b), which was corroborated by the significantly increased phosphorylation of eIF2α in 3D aggregates for bMSCs and ASCs (Figure 4c). The protein expression of eIF2 downstream regulators such as ATF-4, CHOP, and GADD34 was analyzed. GADD34 protein decreased in bMSCs and ASCs following 3D aggregation, which corresponds to the increased ratio of p-eIF2 (Figure 4c,d). Interestingly, ATF-4 protein also decreased while no significant change was observed in the expression CHOP between 3D aggregates and 2D cells in bMSCs and ASCs (Figures 4d and S3b). For the FB group, there was no significant difference between 3D aggregates and 2D cells for all the downstream regulators. Quantitative PCR analysis was performed for both upstream and downstream eIF2 pathway targets: PERK (*EIF2AK3*), eIF2α (*EIF2S1*), eIF2γ (*EIF2S3*), *ATF4*, CHOP (*DDIT3*), and GADD34 (*PPP1R15A*; Figure S3c,d). The downstream target genes *ATF4*, *DDIT3*, and *PPP1R15A* were elevated following 3D aggregation for the three cell types. Similar to our previous study (Bejoy et al., 2019), the ATF-4 and GADD34 upregulation occurs at the messenger RNA level. The rest genes did not show significant differences between 2D and 3D conditions.

3.5 | Small-molecule perturbation of ISR on aggregation-based functional enhancement

To assess the importance of aggregation-induced ISR, salubrinal, a GADD34 inhibitor, and GSK2606414, an inhibitor for the

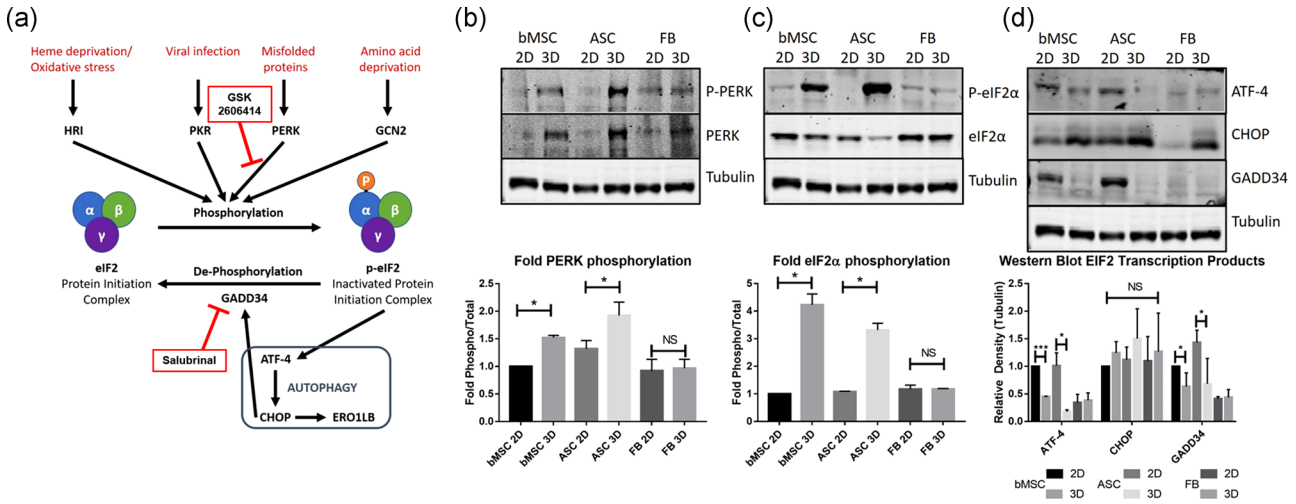

FIGURE 4 Western blot verification of proteomics results and evaluation of aggregation-induced eIF2 pathway activation. (a) During integrated stress response (ISR), eIF2 pathway kinases phosphorylate the alpha subunit which halts protein synthetize and leads to increased autophagy. HRI: the eIF2α kinase heme-regulated inhibitor; PKR: the IFN-induced double-stranded RNA-dependent protein kinase; PERK: protein kinase RNA-like endoplasmic reticulum kinase; GCN2: general control nonderepressible 2, a serine/threonine-protein kinase that senses amino acid deficiency through binding to uncharged transfer RNA. GADD34: the growth arrest and DNA-damaged protein 34, a stress-induced regulatory subunit of the serine/threonine-protein phosphatase 1. (b) Western blot images of PERK, an eIF2 kinase, and the ratio of activation. (c) Western blot readings for activated and total eIF2α along with the ratio of which reflects ISR-based activity. (d) Western blot and densitometry readings of downstream transcription targets of p-eIF2α. Data represent the mean of at least three independent determinations; errors represent the standard error in the mean. eIF2, eukaryotic initiation factor 2. $^*p < .05$ [Color figure can be viewed at wileyonlinelibrary.com]

phosphorylation of PERK, were used to treat the cells under planar and aggregation cultures (Figure S4). Following treatment with salubrinal, planar bMSCs and ASCs showed significantly increased expression of SOX-2, the ratio of p-eIF2α to eIF2α, and activation of autophagy characterized by the ratio of LC3B-II/LC3B-I (Figures 5 and S5). Salubrinal had no significant effect on the bMSC or ASC aggregates. However, FB aggregates showed significantly increased SOX-2 expression with salubrinal treatment. GSK2606414 treatment resulted in a significant reduction in SOX-2 expression for bMSC aggregates and a reduction in the ratio of p-eIF2α to eIF2α for ASC aggregates, but no significant change was observed for any other conditions (Figures 5 and S5).

3.6 | ISR response leads to increased ischemic survival

A major application for MSC therapy is in wound sites as an actuator of anti-inflammation and an initiator of regeneration, which can be enhanced by 3D aggregation (Bhang et al., 2011). To assess the level of ischemic stress response associated with aggregation-induced ISR, planar and aggregated bMSCs, ASCs, and FBs were cultured in (a) normoxia (20% oxygen) with serum and (b) hypoxia (2% oxygen) with serum withdrawal to simulate ischemia. Three-dimensional aggregation significantly increased ischemic survival of bMSCs and ASCs under ischemic environment, while for FB, it decreased survival (Figure 6a). Analysis of caspase activity showed that, for all three cell types, there was a significant increase in caspase 3/7 following aggregation (Figure 6b). Finally, colony-forming unit-fibroblasts (CFU-F) with and without ISR activity was evaluated. Inhibiting ISR (GSK-2606414 treatment) was found to significantly decrease the CFU-F numbers for all three cell types, while locking the ISR (salubrinal treatment) resulted in a smaller yet significant reduction in CFU-F for the FB group, but not affecting bMSCs and ASCs (Figure 6c).

3.7 | Role of biomechanical signaling in aggregation-induced ISR

To reveal the role of biomechanical force in the observed increase in ISR following aggregation, ASCs were treated with Thap, a SERCA agonist that induces endoplasmic reticular calcium release, or 2-APB, which prevents TRP channel Ca^{2+} flux. Western blotting analysis of XBP-1s, ATF-4, CHOP, LC3B-I/II, p-eIF2α, and eIF2α revealed that Thap increased ISR (indicated by phospho-eIF2α) in planar culture but not in aggregates, while 2-APB had no effect on planar cells but resulted in a significant decrease in aggregates (Figure S6a). No significant differences were observed for XBP-1s and ATF-4. For CHOP, Thap treatment increased the protein level for planar cells but not aggregates. The effects of Thap and 2-APB on 2D planar cells and 3D aggregates were clearly seen in the ratio of phospho-eIF2α to total eIF2α (Figure S6b) and in autophagosome synthesis marker, the ratio of LC3B-II to LC3B-I (Figure S6c). Adding Thap resulted in a nearly twofold increase in the ratios of LC3B-I/II, while no significant change

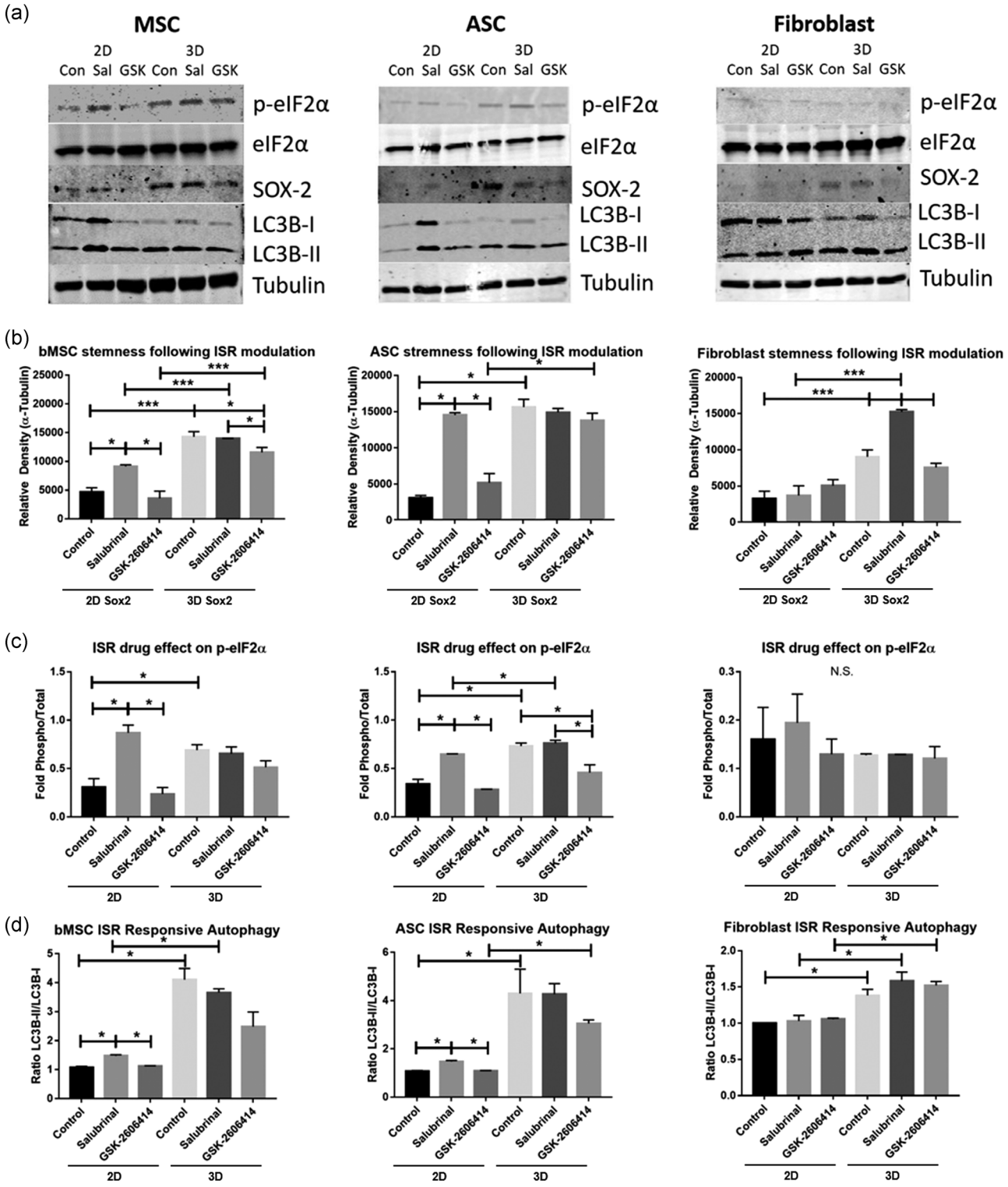

FIGURE 5 Western blot evaluation of stem cell functionality following modulation of integrated stress response (ISR) with small molecules salubrinal and GSK-2606414. (a) Western blot images for bMSCs, ASCs, and FBs. (b) Relative density for protein SOX-2 (i.e., the density of SOX-2 band normalized to the density of α-tubulin band). (c) Fold of phosphorylated eIF2α (p-eIF2α) relative to total eIF2α (i.e., the density of p-eIF2α band divided by the density of eIF2α band), indicating level of ISR response as determined by phosphorylation of eIF2α. (d) Measure of autophasome biogenesis via ratio of LC3B-II/LC3B-I (i.e., the density of LC3B-II band divided by the density of LC3B-I band). Data represent the mean of at least three independent determinations; errors represent the standard error in the mean. ASC, adipose tissue; bMSC, MSCs derived from bone marrow; eIF2, eukaryotic initiation factor 2; FB, fibroblast. $^{*}p < .05$, $^{***}p < .01$

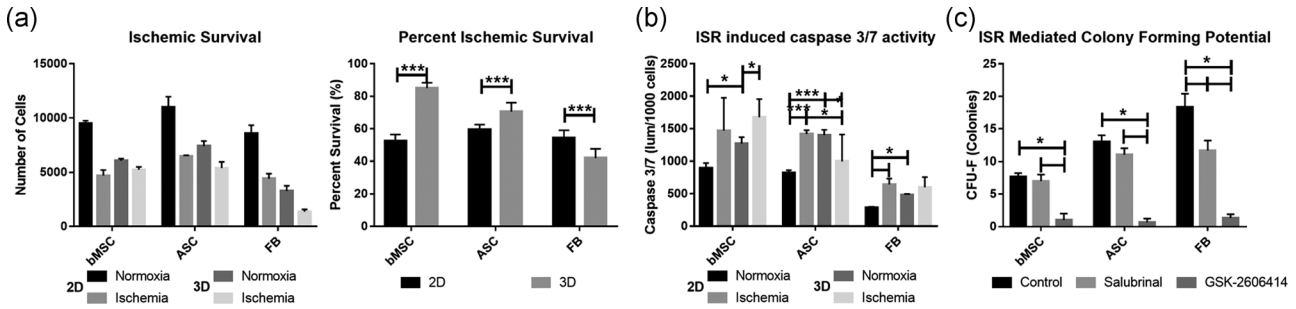

FIGURE 6 Evaluation of how integrated stress response (ISR) affects cellular survival and function. (a) Determination of cellular survival following 24-hr ischemic stress (serum withdrawal and incubation under 2% O_2 tension). (b) Caspase 3/7 activity following ischemic and aggregation culture. (c) Colony-forming unit-fibroblasts (CFU-F) with small-molecule inhibition of ISR for planar cells. Data represent the mean of at least three independent determinations; errors represent the standard error in the mean. $^{*}p < .05$, $^{***}p < .01$

was observed with 2-APB. The opposite trend was observed in aggregates where Thap did not alter either levels, but 2-APB resulted in a significant reduction.

4 | DISCUSSION

The rapid decline of MSC clonogenicity and functional properties following in vitro processing in conjunction with the low cell survival posttransplantation are significant barriers in translation of MSCs to clinical applications (Galipeau & Sensebe, 2018). Identifying the mechanism that regulates the responses of MSCs to external stimuli has important implications in designing optimal expansion and delivery strategies for MSC therapeutic applications (Galipeau & Sensebe, 2018; Yin et al., 2019). MSCs are highly responsive to microenvironmental stimuli arising from biological parameters, for example, immunomodulatory cytokines (Gao et al., 2016; Zhao, Ren, & Han, 2016), biomechanical regulation, for example, culture surface tension or stiffness (Bijonowski et al., 2019; Cesarz, Funnell, Guan, & Tamama, 2016), and physiological modulation, for example, oxygen tension (Hu, Zhao, Wu, & Li, 2019; Peck et al., 2019). Our previous studies have indicated that the significant alterations of MSC aggregates are due to different levels of cortical compaction-induced metabolic reconfiguration rather than hypoxic core within aggregates (Bijonowski et al., 2019; Liu et al., 2017). In fact, at certain size range (100–400 μm), the cells within MSC aggregates have unlimited access to oxygen and no hypoxic core is formed (Bijonowski et al., 2019; Tsai et al., 2017). This study reveals that 3D aggregation of MSCs results in the elevated basal ISR which plays a central role in restoring cellular homeostasis of MSCs and stemness, which enhances the clonogenicity and cell survival under ischemic environment.

4.1 | Proteomics analysis reveals the role of ISR in MSC homeostasis

Previous mass spectrometer-based proteomics analysis of MSCs revealed 463 individual proteins (Foster et al., 2005). In this study, 1,016, 790, and 1,104 proteins in bMSCs, ASCs, and fibroblasts were identified, respectively, which suggest that the extraction and label-free proteomics analysis in our study are more sensitive. Label-free analysis of bone marrow-sourced stem cells has also been utilized previously to study the function of tissues (Han, Hong, & Park, 2019) and in the characterization of cellular responses to chondrogenic treatment regimens (Oswald, Brown, Bulinski, & Hung, 2011). In particular, our PCA results illustrate a significant separation of 2D and 3D samples for the three cell types, bMSCs, ASCs, and fibroblasts.

Upon analysis of the identified proteins, our study discovered that aggregated cells showed fewer proteins than those identified in planar culture for all three cell types. This decrease is likely due to the reduction in protein synthesis per cell following aggregation. Our previous experiments have shown that aggregation reduces the total proteins per cell by 80% (Bijonowski et al., 2019).

Following aggregation of bMSCs and ASCs, it was noted that several ribosomal proteins such as RPL19, RPL12, RPS21, RPS13, and 40S and 60S ribosomal subunits were downregulated in 3D aggregates, all of which are intrinsically linked to biosynthesis and protein homeostasis (Hashem & Frank, 2018; Vatikioti et al., 2019). In addition, downregulation of the subunits of eIF2 complex, eIF2α, and eIF2γ, was observed following 3D aggregation of bMSCs and ASCs, indicating potential involvement of eIF2 signaling pathways in formation of stem cell aggregates. Proteomics analysis lays down a significant case for the activation of ISR following 3D aggregation of bMSCs and ASCs. This observation also indicates a clear difference for handling ISR following aggregation in stem cells compared to somatic cells such as FBs.

4.2 | MSCs exhibit increased ISR activity following aggregation

Normally, an acute ISR would be initiated in response to the existence of misfolded proteins. This cascade of response follows a three-stage cellular event: (a) protein initiation complex eIF2 is inactivated via phosphorylation of the alpha subunit; (b) the misfolded

protein is coated in chaperone proteins that prompt further processing in an attempt to refold or degrade the misfolded proteins; and (c) finally, if the misfolded protein cannot be corrected, proteolysis is activated and the protein is ubiquinated and lysed (Kroemer, Marino, & Levine, 2010). As such, the apparent upregulation in the ISR-associated eIF2 pathway following aggregation of bMSCs and ASCs was very intriguing. Elevated phosphorylation of PERK and eIF2α was observed after aggregation in our study, though ATF-4 protein expression decreased. This seems counter-intuitive since stem cells do utilize the eIF2 pathway to activate ISR and support downstream function (Lee, Gutierrez-Garcia, & Vilchez, 2017; van Galen et al., 2018). Indeed, the activation of the phospho-eIF2 complex attenuates the global protein translation while allowing preferential translation of selected genes such as ATF4, but some stresses do not increase ATF4 despite the robust phosphorylation of eIF2α (Dey et al., 2010). Moreover, it has been recently shown that as stem cells differentiate they accumulate ATF-4, so the reduction in ATF-4 protein may be a sign of preservation of stem cell characteristics (van Galen et al., 2018). GADD34 is responsible for dephosphorylating eIF2α and reinstating protein translation after correcting misfolded proteins (Kroemer et al., 2010). Therefore, the aggregation of stem cells may result in a new protein homeostatic state, with lower level of GADD34 shown in our study (Kratochvilova et al., 2016; Spaan et al., 2019; Young, Palam, Wu, Sachs, & Wek, 2016). CHOP generally follows the changes of its upstream regulator, ATF4 to activate autophagy under stress response (B'Chir et al., 2013). CHOP activation induces cellular apoptosis under prolonged cellular stress (Avivar-Valderas et al., 2011; Matsumoto et al., 2013). However, this study did not observe changes in CHOP in stem cells after aggregation. Thus, though 3D aggregation was considered as external stress, the whole process acts like preconditioning culture to preserve homeostasis and improve stemness for MSCs. Aggregation may induce limited downstream eIF2 pathway activity while maintaining upstream eIF2 and increased autophagy in bMSCs and ASCs. Our previous studies also indicate the increased autophagy in human MSC aggregates (Liu et al., 2017; Tsai, Liu, Yuan, & Ma, 2015; Yuan, Rosenberg, Liu, Grant, & Ma, 2019). Since ATF4-CHOP axis is limited as shown in current study, the potential mechanism of autophagy activation by aggregation needs more investigation.

4.3 | Inhibition of ISR effect prevents aggregation-induced functional enhancement

Modulating the PERK-dependent ISR response arm showed that bMSCs and ASCs rely on aggregation-induced acute ISR to upregulate stemness and restore autophagy (Figure S7). Specifically, it was observed that under 3D aggregation conditions, the levels of SOX-2, the ratio of p-eIF2α to total eIF2α, and LC3B-II/LC3B-I were significantly increased for bMSCs and ASCs. To further pinpoint the role of aggregation-induced ISR, inhibition of key steps of PERK-eIF2 axis was performed. Salubrinal did not show the influence for bMSC and ASC aggregates, which may indicate that aggregation results in a new heightened homeostatic activation. However, increasing the phosphorylation of eIF2α via inhibition of GADD34 by Salubrinal increased SOX-2, which illustrates a "rescue" effect upon activation of ISR, similar to what has been achieved by others upon reactivating ISR (van Galen et al., 2018) or autophagy (Pennock et al., 2015). This was further corroborated by the reduction in SOX-2 in bMSCs and p-eIF2α for ASCs after GSK2606414 treatment as shown in this study. Therefore, inhibition of PERK phosphorylation via GSK-2606414 attenuates the effects of eIF2 and ISR in stem cells following aggregation to a certain degree. It is noted that FBs did not respond to any of the inhibition significantly except for SOX-2 expression, which may indicate that FBs adapt to cellular stress and regulate ISR in a different manner. Similar trends were observed for functional evaluation and survival under ischemic stress. Together, the responses of bMSCs and ASCs following GSK-2606414 and salubrinal treatment corroborate our hypothesis that aggregation-induced ISR is responsible for stem cell functional recovery.

4.4 | ISR helps manage environmental stressors and extends stem cell potential

The therapeutic potential of MSCs is associated with their ability to moderate the regenerative niche in a wound site, which commonly involves an ischemic environment (Bhang et al., 2011; Chen et al., 2016; Sarmah et al., 2018). This study observed that both bMSCs and ASCs showed significantly increased survival following 3D aggregation in the ischemic environment, while the opposite effect was seen in FB. Similar findings were observed in an in vivo study, which reported that aggregation improved engraftment and survival of MSCs following injection into ischemic injured rat kidneys (Xu, Shi, Xu, & Zhang, 2016) and brain (Yuan et al., 2019). Interestingly, significantly increased caspase 3/7 activity was observed in aggregates which result in increased cellular apoptosis. This increase in caspase activity was also observed previously by our group (Tsai et al., 2015) and others (Bazhanov et al., 2016; Cesarz et al., 2016). The increased ISR activity has previously been shown to increase caspase 3/7 activity and regulate the apoptosis instead of necrosis (Young et al., 2016). Finally, the effect of ISR on stem cell content was evaluated utilizing CFU-F activity. As expected, inhibiting phosphorylation of PERK via GSK-2606414 decreased CFU-F numbers for all three cell types. In addition, a significantly smaller reduction following salubrinal treatment was observed. Preventing the resolution in the eIF2 pathway would prevent the protein synthesis necessary for cellular replication (Kroemer et al., 2010). Due to inherent ISR response in bMSCs and ASCs following 3D aggregation, the cells are able to adapt to ischemic culture and to the innate ISR required for colony formation.

4.5 | Calcium signaling is required for aggregation-induced ISR

Calcium signaling is an important aspect of cellular homeostasis and it is known that Ca^{2+} plays an important role in ISR signaling, as the

release of accumulation of misfolded proteins signals from endoplasmic reticulum rely on calcium storage and signaling (Stutzmann & Mattson, 2011). Therefore, our study investigated the role of biomechanical-induced calcium signaling changes in ISR activation. When cytosolic calcium was increased via Thap treatment, a significant increase in the ratio of phospho-eIF2α to total eIF2α was observed for planar cells but not aggregate cells, and a similar trend was observed for the ratio of LC3B-II to LC3B-I. This observation is likely due to the increase in cytosolic calcium following aggregation. Treatment with 2-APB blocked store-operated Ca^{2+} entry and significantly reduced the ratios of phospho-eIF2α to eIF2α and LC3B-II to LC3B-I following aggregation, showing the important role of calcium signaling in the aggregation-induced ISR.

5 | CONCLUSIONS

This study sets out to assess how ISR affects MSC stemness and homeostatic state following 3D aggregation. Proteomics analysis identified the eIF2 pathway as the dominant pathway. In addition, chaperone content and proteasome proteins were shifted following aggregation, which may underlie other ISR-based cellular events. Western blot validated that the eIF2 pathway was activated in bMSCs and ASCs, while not in fully differentiated dermal fibroblasts. The downstream effect was analyzed with small molecules, and the improvements in cellular autophagy and stemness after aggregation were shown to be ISR-dependent. MSC survival under ischemic condition was also shown to be ISR-dependent, with fibroblasts showing reduced efficacy following aggregation. This study provides details on preconditioning MSCs via aggregation and the important role of heightened ISR in stem cells for re-establishing homeostasis and preserving stemness. The results of this study are significant for MSC biomanufacturing and clinical applications to achieve a better therapeutic outcome.

ACKNOWLEDGMENTS

This study was supported by the National Science Foundation (CBET #1743426) and the National Institutes of Health (R01NS102395-01A1). The authors would like to thank the Translational Science Laboratory of Florida State University for their kind help in proteomic data analysis, and Dr Brian Washburn and Kristina Poduch of FSU Department of Biomedical Sciences for performing qRT-PCR experiments. The content is solely the responsibility of the authors and does not necessarily represent the official views of the National Institutes of Health.

CONFLICT OF INTERESTS

The authors declare that there are no conflict of interests.

ORCID

Brent M. Bijonowski http://orcid.org/0000-0002-9906-9176
Yan Li http://orcid.org/0000-0002-5938-8519

REFERENCES

Avivar-Valderas, A., Salas, E., Bobrovnikova-Marjon, E., Diehl, J. A., Nagi, C., Debnath, J., & Aguirre-Ghiso, J. A. (2011). PERK integrates autophagy and oxidative stress responses to promote survival during extracellular matrix detachment. *Molecular and Cellular Biology*, *31*, 3616–3629.

von Bahr, L., Sundberg, B., Lonnies, L., Sander, B., Karbach, H., Hagglund, H., … Ringden, O. (2012). Long-term complications, immunologic effects, and role of passage for outcome in mesenchymal stromal cell therapy. *Biology of Blood and Marrow Transplantation*, *18*, 557–564.

Banfi, A., Muraglia, A., Dozin, B., Mastrogiacomo, M., Cancedda, R., & Quarto, R. (2000). Proliferation kinetics and differentiation potential of ex vivo expanded human bone marrow stromal cells: Implications for their use in cell therapy. *Experimental Hematology*, *28*, 707–715.

Bazhanov, N., Ylostalo, J. H., Bartosh, T. J., Tiblow, A., Mohammadipoor, A., Foskett, A., & Prockop, D. J. (2016). Intraperitoneally infused human mesenchymal stem cells form aggregates with mouse immune cells and attach to peritoneal organs. *Stem Cell Research & Therapy*, *7*, 27.

B'Chir, W., Maurin, A. C., Carraro, V., Averous, J., Jousse, C., Muranishi, Y., … Bruhat, A. (2013). The eIF2alpha/ATF4 pathway is essential for stress-induced autophagy gene expression. *Nucleic Acids Research*, *41*, 7683–7699.

Bejoy, J., Yuan, X., Song, L., Hua, T., Jeske, R., Sart, S., … Li, Y. (2019). Genomics analysis of metabolic pathways of human stem cell-derived microglia-like cells and the integrated cortical spheroids. *Stem Cells International*, *2019*, 2382534.

Bhang, S. H., Cho, S.-W., La, W.-G., Lee, T.-J., Yang, H. S., Sun, A.-Y., … Kim, B.-S. (2011). Angiogenesis in ischemic tissue produced by spheroid grafting of human adipose-derived stromal cells. *Biomaterials*, *32*, 2734–2747.

Bianco, P., Robey, P. G., Saggio, I., & Riminucci, M. (2010). "Mesenchymal" stem cells in human bone marrow (skeletal stem cells): A critical discussion of their nature, identity, and significance in incurable skeletal disease. *Human Gene Therapy*, *21*, 1057–1066.

Bijonowski, B. M., Daraiseh, S. I., Yuan, X., & Ma, T. (2019). Size-dependent cortical compaction induces metabolic adaptation in mesenchymal stem cell aggregates. *Tissue Engineering, Part A*, *25*, 575–587.

Cesarz, Z., Funnell, J. L., Guan, J., & Tamama, K. (2016). Soft elasticity-associated signaling and bone morphogenic protein 2 are key regulators of mesenchymal stem cell spheroidal aggregates. *Stem Cells and Development*, *25*, 622–635.

Chamberlain, G., Fox, J., Ashton, B., & Middleton, J. (2009). Concise review: Mesenchymal stem cells—Their phenotype, differentiation capacity, immunological features, and potential for homing. *Stem Cells*, *25*, 2739–2749.

Chen, K.-H., Chen, C.-H., Wallace, C. G., Yuen, C.-M., Kao, G.-S., Chen, Y.-L., … Yip, H.-K. (2016). Intravenous administration of xenogenic adipose-derived mesenchymal stem cells (ADMSC) and ADMSC-derived exosomes markedly reduced brain infarct volume and preserved neurological function in rat after acute ischemic stroke. *Oncotarget*, *46*, 74537–74556.

Costa, M. H., McDevitt, T. C., Cabral, J. M., da Silva, C. L., & Ferreira, F. C. (2017). Tridimensional configurations of human mesenchymal stem/stromal cells to enhance cell paracrine potential towards wound healing processes. *Journal of Biotechnology*, *262*, 28–39.

Das, R. K., Gocheva, V., Hammink, R., Zouani, O. F., & Rowan, A. E. (2016). Stress-stiffening-mediated stem-cell commitment switch in soft responsive hydrogels. *Nature Materials*, *15*, 318–325.

Dey, S., Baird, T. D., Zhou, D., Palam, L. R., Spandau, D. F., & Wek, R. C. (2010). Both transcriptional regulation and translational control of ATF4 are central to the integrated stress response. *Journal of Biological Chemistry*, *285*, 33165–33174.

Diaz, M. F., Vaidya, A. B., Evans, S. M., Lee, H. J., Aertker, B. M., Alexander, A. J., … Wenzel, P. L. (2017). Biomechanical forces promote

immune regulatory function of bone marrow mesenchymal stromal cells. *Stem Cells*, *35*, 1259–1272.

Foster, L. J., Zeemann, P. A., Li, C., Mann, M., Jensen, O. N., & Kassem, M. (2005). Differential expression profiling of membrane proteins by quantitative proteomics in a human mesenchymal stem cell line undergoing osteoblast differentiation. *Stem Cells*, *23*, 1367–1377.

Fung, M., Yuan, Y., Atkins, H., Shi, Q., & Bubela, T. (2017). Responsible translation of stem cell research: an assessment of clinical trial registration and publications. *Stem Cell Reports*, *8*, 1190–1201.

van Galen, P., Mbong, N., Kreso, A., Schoof, E. M., Wangenblast, E., Ng, S. W., … Dick, J. E. (2018). Integrated stess response activity marks stem cells in normal hematopoiesis and leukemia. *Cell Reports*, *25*, 1109–1117.

Galipeau, J., & Sensebe, L. (2018). Mesenchymal stromal cells: Clinical challenges and therapeutic opportunitites. *Stem Cells*, *22*, 824–833.

Gao, F., Chiu, S., Motan, D., Zhang, Z., Chen, L., Ji, H.-L., … Lian, Q. (2016). Mesenchymal stem cells and immunomodulation: Current status and future prospects. *Cell Death & Disease*, *7*, e2062.

Garcia-Prat, L., Martinez-Vicente, M., Perdiguero, E., Ortet, L., Rodriguez-Ubreva, J., Rebollo, E., … Munoz-Canoves, P. (2016). Autophagy maintanins stemness by preventing senescence. *Nature*, *529*, 37–42.

Han, N.-Y., Hong, J.-Y., & Park, J.-M. (2019). Label-free quantitative proteomic analysis of human periodontal ligament stem cells by high-resolution mass spectrometry. *Journal of Periodontal Research*, *54*, 53–62.

Hashem, Y., & Frank, J. (2018). The Jigsaw puzzle of mRNA translation initiation in eukaryotes: A decade of structures unraveling the mechanics of the process. *Annual Review of Biophysics*, *47*, 125–151.

Hu, C., Zhao, L., Wu, D., & Li, L. (2019). Modulating autophagy in mesenchymal stem cells effectively protects against hypoxia- or ischemia-induced injury. *Stem Cell Research & Therapy*, *10*, 120.

Khong, D., Li, M., Singleton, A., Chin, L.-Y., Mukundan, S., & Parekkadan, B. (2018). Orthogonal potency analysis of mesenchymal stromal cell function during ex vivo expansion. *Experimental Cell Research*, *362*, 102–110.

Kratochvilova, K., Moran, L., Padourova, S., Stejskal, S., Tesarova, L., Simara, P., … Vanhara, P. (2016). The role of the endoplasmic reticulum stress in stemness, pluripotency and development. *European Journal of Cell Biology*, *95*, 115–123.

Kroemer, G., Marino, G., & Levine, B. (2010). Autophagy and the Integrated Stress Response. *Molecular Cell*, *40*, 280–293.

Lee, H. J., Gutierrez-Garcia, R., & Vilchez, D. (2017). Embryonic stem cells: A novel paradigm to study proteostasis? *FEBS Journal*, *284*, 391–398.

Liu, Y., Munoz, N., Tsai, A.-C., Logan, T. M., & Ma, T. (2017). Metabolic reconfiguration supports reacquisition of primitive phenotype in human mesenchymal stem cell aggregates. *Stem Cells*, *35*, 398–410.

Lu, P. D., Harding, H. P., & Ron, D. (2004). Translation reinitiation at alternative open reading frames regulates gene expression in an integrated stress response. *Journal of Cell Biology*, *167*, 27–33.

Matsumoto, H., Miyazaki, S., Matsuyama, S., Takeda, M., Kawano, M., Nakagawa, H., … Matsuo, S. (2013). Selection of autophagy or apoptosis in cells exposed to ER-stress depends on ATF4 expression pattern with or without CHOP expression. *Biology Open*, *2*, 1084–1090.

Murphy, M. B., Moncivais, K., & Caplan, A. I. (2013). Mesenchymal stem cells: Environmentally responsive therapeutics for regenerative medicine. *Experimental & Molecular Medicine*, *45*, e54.

Oswald, E. S., Brown, L. M., Bulinski, J. C., & Hung, C. T. (2011). Label-free protein profiling of adipose-derived human stem cells under hyperosmotic treatment. *Journal of Proteome Research*, *10*, 3050–3059.

Pakos-Zebrucka, K., Koryga, I., Mnich, K., Ljujic, M., Samali, A., & Gorman, A. M. (2016). The integrated stress response. *EMBO Reports*, *17*, 1374–1395.

Peck, S. H., Bendigo, J. R., Tobias, J. W., Dodge, G. R., Malhotra, N. R., Mauck, R. L., & Smith, L. J. (2019). Hypoxic preconditioning enhances bone marrow-derived mesenchymal stem cell survival in a low oxygen and nutrient-limited 3D microenvironment. *Cartilage*, https://doi.org/10.1177/1947603519841675

Pennock, R., Bray, E., Pryor, P., James, S., McKeegan, P., Sturmey, R., & Genever, P. (2015). Human cell dedifferentiation in mesenchymal condensates through controlled autophagy. *Scientific Reports*, *5*, 13113.

Sarmah, D., Agrawal, V., Rane, P., Bhute, S., Watanabe, M., Kalia, K., … Bhattacharya, P. (2018). Mesenchymal stem cell therapy in ischemic stroke: A meta-analysis of preclinical studies. *Clinical Pharmacology and Therapeutics*, *103*, 990–998.

Sart, S., Tomasi, R. F., Barizien, A., Amselem, G., Cumano, A., & Baroud, C. N. (2020). Mapping the structure and biological functions within mesenchymal bodies using microfluidics. *Science Advances*, *6*, eaaw7853.

Sart, S., Tsai, A.-C., Li, Y., & Ma, T. (2014). Three-dimensional aggregates of mesenchymal stem cells: Cellular mechanisms, biological properties, and applications. *Tissue Engineering, Part B Reviews*, *20*, 365–380.

Searfoss, G. H., Paisley, B. M., Goldstein, K. M., Baker, T. K., & Willy, J. A. (2019). The integrated stress response regulates cell health of cardiac progenitors. *Toxicological Sciences*, *167*, 202–210.

Song, W.-J., Li, Q., Ryu, M.-O., Ahn, J.-O., Bhang, D. H., Jung, Y. C., & Youn, H.-Y. (2017). TSG-6 secreted by human adipose tissue-derived mesenchymal stem cells ameliorates DSS-induced colitis by inducing M2 macrophage polarization in mice. *Scientific Reports*, *7*, 5197.

Spaan, C. N., Smit, W. L., van Lidth de Jeude, J. F., Meijer, B. J., Muncan, V., van den Brink, G. R., & Heijmans, J. (2019). Expression of UPR effector proteins ATF6 and XBP1 reduce colorectal cancer cell proliferation and stemness by activating PERK signaling. *Cell Death & Disease*, *10*, 490.

Stutzmann, G. E., & Mattson, M. P. (2011). Endoplasmic reticulum Ca2+ handling in excitable cells in health and disease. *Pharmacological Reviews*, *63*, 700–727.

Tsai, A.-C., Liu, Y., Yuan, X., Chella, R., & Ma, T. (2017). Aggregation kinetics of human mesenchymal stem cells under wave motion. *Biotechnology Journal*, *12*, 1600448.

Tsai, A.-C., Liu, Y., Yuan, X., & Ma, T. (2015). Compaction, fusion, and functional activation of three-dimensional human mesenchymal stem cell aggregate. *Tissue Engineering, Part A*, *21*, 1705–1719.

Wang, Y., Chen, X., Cao, W., & Shi, Y. (2014). Plasticity of mesenchymal stem cells in immunomodulation: Pathological and therapeutic implications. *Nature Immunology*, *15*, 1009–1016.

Wisniewski, J. R., Zougman, A., Nagaraj, N., & Mann, M. (2009). Universal sample preparation method for proteome analysis. *Nature Methods*, *6*, 359–362.

Wobma, H. M., Liu, D., & Vunjak-Novakovic, G. (2018). Paracrine effects of mesenchymal stromal cells cultured in three-dimensional settings on tissue repair. *ACS Biomaterials Science & Engineering*, *4*, 1162–1175.

Xu, Y., Shi, T., Xu, A., & Zhang, L. (2016). 3D spheroid culture enhances survival and therapeutic capacities of MSCs injected into ischemic kidney. *Journal of Cellular and Molecular Medicine*, *20*, 1202–1213.

Yin, J. Q., Zhu, J., & Ankrum, J. A. (2019). Manufacturing of primed mesenchymal stromal cells for therapy. *Nature Biomedical Engineering*, *3*, 90–104.

Young, S. K., Palam, L. R., Wu, C., Sachs, M. S., & Wek, R. C. (2016). Ribosome elongation stall directs gene-specific translation in the integrated stress response. *Journal of Biological Chemistry*, *291*, 6546–6558.

Yuan, X., Rosenberg, J. T., Liu, Y., Grant, S. C., & Ma, T. (2019). Aggregation of human mesenchymal stem cells enhances survival and efficacy in stroke treatment. *Cytotherapy*, *21*, 1033–1048.

Zhao, Q., Ren, H., & Han, Z. (2016). Mesenchymal stem cells: Immunomodulatory capability and clinical potential in immune diseases. *Journal of Cellular Immunotherapy*, *2*, 3–20.

SUPPORTING INFORMATION

Additional supporting information may be found online in the Supporting Information section.

How to cite this article: Bijonowski BM, Fu Q, Yuan X, et al. Aggregation-induced integrated stress response rejuvenates culture-expanded human mesenchymal stem cells. *Biotechnology and Bioengineering*. 2020;117:3136–3149. https://doi.org/10.1002/bit.27474